Broad-spectrum in vitro antiviral activity of ODBG-P-RVn: an orally-available, lipid-modified monophosphate prodrug of remdesivir parent nucleoside (GS-441524)

Michael K. Lo[a*]#, Punya Shrivastava-Ranjan[a], Payel Chatterjee[a], Mike Flint[a], James R. Beadle[b], Nadejda Valiaeva[b], Robert T. Schooley[b], Karl Y. Hostetler[b], Joel M. Montgomery[a], and Christina Spiropoulou[a*]

[a]Viral Special Pathogens Branch, Centers for Disease Control and Prevention, Department of Health and Human Services, Atlanta, Georgia, USA

[b]Division of Infectious Diseases and Global Public Health, Department of Medicine, University of California San Diego, La Jolla, California, USA

Running title: Antiviral potency of lipid-modified remdesivir nucleoside

*Address correspondence to:

#Michael K. Lo: mko2@cdc.gov and Christina F. Spiropoulou: ccs8@cdc.gov

KEYWORDS: SARS-CoV-2, Ebola virus, Nipah virus, respiratory viruses, hemorrhagic fever virus, filovirus, paramyxovirus, henipavirus, Remdesivir, GS-5734, Remdesivir nucleoside, GS-441524, antiviral agents, lipid prodrugs, ODBG, Vero E6 cells, Huh7 cells, NCI-H358 cells, human telomerase reverse-transcriptase (hTERT) immortalized microvascular endothelial cells (TIME), and human small airway epithelial cells (HSAEC1-KT)

ABSTRACT

The intravenous administration of remdesivir for COVID-19 confines its utility to hospitalized patients. We evaluated the broad-spectrum antiviral activity of ODBG-P-RVn, an orally available, lipid-modified monophosphate prodrug of the remdesivir parent nucleoside (GS-441524) against viruses that cause diseases of human public health concern, including SARS-CoV-2. ODBG-P-RVn showed 20-fold greater antiviral activity than GS-441524 and had near-equivalent activity to remdesivir in primary-like human small airway epithelial cells. Our results warrant investigation of ODBG-P-RVn efficacy in vivo.

29 Remdesivir (RDV; Veklury, GS-5734) is an adenosine nucleotide analog phosphoramidate prodrug with
30 broad-spectrum antiviral activity in vitro and in vivo (1-8), and is currently the only therapeutic approved
31 by the FDA for treating coronavirus 19 disease (COVID-19) in hospitalized patients over the age of 12 (9).
32 While RDV did not significantly reduce COVID-19 mortality, it did shorten the time to recovery compared
33 to a placebo control group (10). The short half-life of RDV in human and animal plasma (1, 8, 11, 12),
34 alongside the in vivo efficacy of RDV parent nucleoside (GS-441524, RVn) against coronaviruses including
35 severe acute respiratory syndrome coronavirus 2 (SARS-CoV-2) (13-16), have driven proposals to utilize
36 RVn instead of RDV to treat COVID-19 (17). A recent comparative pharmacokinetic study in non-human
37 primates, however, demonstrated higher nucleoside triphosphate (NTP) levels in lower respiratory tract
38 tissues of RDV-dosed animals than in RVn-dosed animals (8). A significant drawback of RDV is the
39 requirement for intravenous administration, which limits its use to hospital contexts. In an attempt to
40 develop an orally bioavailable form of remdesivir, we recently synthesized a 1-O-octadecyl-2-O-benzyl-
41 sn-glycerylester (ODBG) lipid-modified monophosphate prodrug of RVn (ODBG-P-RVn), which
42 demonstrated more favorable in vitro antiviral activity against SARS-CoV-2 compared to that of RVn and
43 RDV in Vero-E6 cells (18).

44 In this study, we extended our in vitro comparisons to include 14 viruses from across 7 virus families
45 responsible for causing diseases of significant human public health concern. These were *Filoviridae*:
46 Ebola virus (EBOV) and Marburg virus (MARV) (19, 20); *Paramyxoviridae*: Nipah virus (NiV), Hendra virus
47 (HeV), human parainfluenza virus 3 (hPIV3), measles virus (MV), mumps virus (MuV), and Sosuga virus
48 (SoSuV) (21-27); *Pneumoviridae*: respiratory syncytial virus (RSV) (28); *Flaviviridae*: yellow fever virus
49 (YFV); *Arenaviridae*: Lassa virus (LASV) (29); *Nairoviridae*: Crimean-Congo hemorrhagic fever virus
50 (CCHFV) (30); and *Coronaviridae*: SARS-CoV-2 (31). We utilized 3 previously described assays to compare
51 the antiviral activities of RVn, RDV, and ODBG-P-RVn against this panel of viruses: 1) directly measuring
52 fluorescence of a reporter protein expressed by recombinant viruses (REP) (2), (Figure 1A); 2)

53 quantitating focus-forming units (FFU) via fluorescent reporter imaging (32) (Figure 1B); and 3) indirectly
54 measuring cytopathic effect (CPE) based on cellular ATP levels (CellTiterGlo 2.0, Promega) (2) (Figure
55 1C), which was also used to evaluate compound cytotoxicity (Figure 1D). Assay conditions varied based
56 on virus replication kinetics and on the specific assay used; multiplicities of infection (MOI) ranged from
57 0.01–0.25, and endpoint measurements were conducted between 72-144 hours post-infection (hpi). We
58 initially conducted dose-response experiments using 8-point, 3-fold serial dilutions of RVn, RDV, and
59 ODBG-P-RVn against our panel of viruses in Vero-E6 cells, and showed that ODBG-P-RVn consistently
60 had greater antiviral activity than RVn and RDV against all viruses susceptible to RVn/RDV inhibition,
61 with effective concentration (EC_{50}) values ranging from 0.026 to 1.13 µM (Figure 1, Vero-E6 assays
62 represented in left column of panels A, B, C; Supplemental Figure S1; Table 1). RVn and ODBG-P-RVn
63 induced partial cytotoxicity but only at the highest concentration tested (100 µM) and without reaching
64 50% cytotoxicity (CC_{50}). We then compared these antivirals in human hepatoma (Huh7) and
65 bronchioalveolar carcinoma (NCI-H358) cell lines, which represent more relevant cell types targeted by
66 subsets of viruses used in our study. In both human cell lines, although ODBG-P-RVn showed EC_{50} values
67 remarkably similar to those observed in Vero-E6 cells and was 3- to 5-fold more active than RVn, it
68 consistently showed 6- to 20-fold less activity than RDV (Figure 1 [Huh7 and NCI-H358 assays
69 represented, respectively, in the middle and right columns of panels A, B, and C]; Supplemental Figures
70 S2, S3; Table 1). Whereas CC_{50} values for RDV in Huh7 and NCI-H358 cells were 54.2 and 77.2 µM,
71 respectively, ODBG-P-RVn was less cytotoxic in Huh7 cells (CC_{50} = 93.4 µM) and did not show
72 measurable cytotoxicity in NCI-H358 cells even at the highest concentration tested (100 µM) (Figure 1D,
73 right panel; Table 1).

74 To further evaluate cell type-specific effects on the antiviral activities of RVn, RDV, and ODBG-P-RVn, we
75 tested them against a smaller subset of filoviruses (EBOV-ZsG, MARV-ZsG) and a paramyxovirus (NiV-
76 ZsG) expressing ZsGreen reporter in primary-like human telomerase reverse transcriptase (hTERT)

77 immortalized human microvascular endothelial (TIME) cells (33, 34). In TIME cells, we observed a similar
78 trend in antiviral activity as in Huh7 and NCI-H358 cells, with ODBG-P-RVn showing 15- to 22-fold
79 greater activity than RVn, but 5- to 8-fold less activity than RDV in reporter-based assays (Figure 2A,
80 Table 2). To confirm this, we compared the respective abilities of RDV and ODBG-P-RVn to reduce
81 infectious yield of EBOV-ZsG and NiV-ZsG (MOI = 0.25) when cells were treated with each compound 2
82 hpi. Virus supernatants were collected at 72hpi and titered on Huh7 (for EBOV-ZsG) or NCI-H358 (for
83 NiV-ZsG) cells to determine 50% tissue culture infectious dose ($TCID_{50}$) by the method of Reed and
84 Muench (35). Both RDV and ODBG-P-RVn equivalently reduced infectious yield of EBOV-ZsG by up to 4
85 $\log_{10}$ and of NiV-ZsG by approximately 2 $\log_{10}$, in a dose-dependent manner, with EC_{50} values closely
86 mirroring values determined in reporter assays (Figure 2B, left and middle panels; Table 2). However,
87 RDV was more cytotoxic (CC_{50} = 17.2 μM) than ODBG-P-RVn (CC_{50} > 50 μM) (Figure 2B, right panel; Table
88 2), which is reflected in its biphasic inhibition of NiV-ZsG (Figure 2B, middle panel, cytotoxic inhibition by
89 RDV shown at 16.6 μM). Since the ODBG lipid modification has been shown to enhance in vivo lung
90 tissue distribution for a different orally administered nucleoside (36), we compared the activity of the 3
91 compounds against filoviruses, paramyxoviruses, and RSV in another primary-like, hTERT-immortalized
92 small airway epithelial cell (HSAEC1-KT) (37). Notably, the dose-response curves of RDV and ODBG-P-
93 RVn were strikingly similar, with EC_{50} values in the submicromolar range within a 3-fold range of each
94 other; EC_{50} values for some viruses were almost identical (Figure 2C; Supplemental Figure 4; Table 2).
95 Furthermore, RDV and ODBG-P-RVn equivalently reduced the infectious yields of EBOV-ZsG and NiV-ZsG
96 in HSAEC1-KT cells by by 5 $\log_{10}$ and 3 $\log_{10}$, respectively, and their EC_{50} values reflected the limited
97 differential in antiviral activity between them (Figure 2D, left and middle panels; Table 2). Although
98 ODBG-P-RVn was more cytotoxic (CC_{50} = 20.5) in HSAEC1-KT cells than RDV (CC_{50} > 100; Figure 2D, right
99 panel; Table 2), it also effectively reduced virus yields at non-cytotoxic concentrations.

100 In summary, our results demonstrate that ODBG-P-RVn has greater antiviral activity than RVn in all cell
101 lines tested and has cell-type dependent activity levels that range from moderately lesser than to nearly
102 equal to those of RDV. *In vivo* RDV is converted rapidly to RVn (1, 8, 11, 12), which has 0.5 to 2 $\log_{10}$ less
103 activity than RDV against most of the viruses tested. In contrast, ODBG-P-RVn is stable in plasma for >24
104 hours and at therapeutic plasma levels of ODBG-P-Rvn (above EC_{90} for SARS-CoV-2) after oral
105 administration of 16.9 mg/kg to Syrian hamsters; furthermore RVn was not observed at virologically
106 significant levels (38). Thus, one would predict sustained *in vivo* antiviral activity with ODBG-P-RVn
107 without substantial generation in plasma of RVn, the less active metabolite. Taken together, our results
108 strongly support investigation of in vivo efficacy of ODBG-P-RVn not only against SARS-CoV-2 but also
109 against other viruses significant to human health.

110 ACKNOWLEDGMENTS

111 We thank Tatyana Klimova for helpful comments in reviewing the manuscript. We thank Pei-Yong Shi
112 (University of Texas Medical Branch) for the kind gift of the reporter SARS-CoV-2 expressing
113 mNeonGreen. The findings and conclusions in this report are those of the authors and do not necessarily
114 represent those of the Centers for Disease Control and Prevention. This work was supported by CDC
115 core funding and by the National Institute of Allergy and Infectious Diseases (RO1-AI131424).

116 References

117 1. Warren TK, Jordan R, Lo MK, Ray AS, Mackman RL, Soloveva V, Siegel D, Perron M, Bannister R,
118 Hui HC, Larson N, Strickley R, Wells J, Stuthman KS, Van Tongeren SA, Garza NL, Donnelly G,
119 Shurtleff AC, Retterer CJ, Gharaibeh D, Zamani R, Kenny T, Eaton BP, Grimes E, Welch LS, Gomba
120 L, Wilhelmsen CL, Nichols DK, Nuss JE, Nagle ER, Kugelman JR, Palacios G, Doerffler E, Neville S,
121 Carra E, Clarke MO, Zhang L, Lew W, Ross B, Wang Q, Chun K, Wolfe L, Babusis D, Park Y, Stray
122 KM, Trancheva I, Feng JY, Barauskas O, Xu Y, Wong P, et al. 2016. Therapeutic efficacy of the
123 small molecule GS-5734 against Ebola virus in rhesus monkeys. Nature 531:381-5.
124 2. Lo MK, Jordan R, Arvey A, Sudhamsu J, Shrivastava-Ranjan P, Hotard AL, Flint M, McMullan LK,
125 Siegel D, Clarke MO, Mackman RL, Hui HC, Perron M, Ray AS, Cihlar T, Nichol ST, Spiropoulou CF.
126 2017. GS-5734 and its parent nucleoside analog inhibit Filo-, Pneumo-, and Paramyxoviruses. Sci
127 Rep 7:43395.
128 3. Sheahan TP, Sims AC, Graham RL, Menachery VD, Gralinski LE, Case JB, Leist SR, Pyrc K, Feng JY,
129 Trantcheva I, Bannister R, Park Y, Babusis D, Clarke MO, Mackman RL, Spahn JE, Palmiotti CA,
130 Siegel D, Ray AS, Cihlar T, Jordan R, Denison MR, Baric RS. 2017. Broad-spectrum antiviral GS-
131 5734 inhibits both epidemic and zoonotic coronaviruses. Sci Transl Med 9.
132 4. Lo MK, Feldmann F, Gary JM, Jordan R, Bannister R, Cronin J, Patel NR, Klena JD, Nichol ST, Cihlar
133 T, Zaki SR, Feldmann H, Spiropoulou CF, de Wit E. 2019. Remdesivir (GS-5734) protects African
134 green monkeys from Nipah virus challenge. Sci Transl Med 11.
135 5. de Wit E, Feldmann F, Cronin J, Jordan R, Okumura A, Thomas T, Scott D, Cihlar T, Feldmann H.
136 2020. Prophylactic and therapeutic remdesivir (GS-5734) treatment in the rhesus macaque
137 model of MERS-CoV infection. Proc Natl Acad Sci U S A doi:10.1073/pnas.1922083117.
138 6. Pruijssers AJ, George AS, Schafer A, Leist SR, Gralinksi LE, Dinnon KH, 3rd, Yount BL, Agostini ML,
139 Stevens LJ, Chappell JD, Lu X, Hughes TM, Gully K, Martinez DR, Brown AJ, Graham RL, Perry JK,
140 Du Pont V, Pitts J, Ma B, Babusis D, Murakami E, Feng JY, Bilello JP, Porter DP, Cihlar T, Baric RS,
141 Denison MR, Sheahan TP. 2020. Remdesivir Inhibits SARS-CoV-2 in Human Lung Cells and
142 Chimeric SARS-CoV Expressing the SARS-CoV-2 RNA Polymerase in Mice. Cell Rep 32:107940.
143 7. Sheahan TP, Sims AC, Leist SR, Schafer A, Won J, Brown AJ, Montgomery SA, Hogg A, Babusis D,
144 Clarke MO, Spahn JE, Bauer L, Sellers S, Porter D, Feng JY, Cihlar T, Jordan R, Denison MR, Baric
145 RS. 2020. Comparative therapeutic efficacy of remdesivir and combination lopinavir, ritonavir,
146 and interferon beta against MERS-CoV. Nat Commun 11:222.
147 8. Mackman RL, Hui HC, Perron M, Murakami E, Palmiotti C, Lee G, Stray K, Zhang L, Goyal B, Chun
148 K, Byun D, Siegel D, Simonovich S, Du Pont V, Pitts J, Babusis D, Vijjapurapu A, Lu X, Kim C, Zhao
149 X, Chan J, Ma B, Lye D, Vandersteen A, Wortman S, Barrett KT, Toteva M, Jordan R, Subramanian
150 R, Bilello JP, Cihlar T. 2021. Prodrugs of a 1-CN-4-Aza-7,9-dideazaadenosine C-Nucleoside
151 Leading to the Discovery of Remdesivir (GS-5734) as a Potent Inhibitor of Respiratory Syncytial
152 Virus with Efficacy in the African Green Monkey Model of RSV. Journal of Medicinal Chemistry
153 64:5001-5017.
154 9. Gilead. 2020. https://www.veklury.com/. Accessed 07/08/2021.
155 10. Beigel JH, Tomashek KM, Dodd LE, Mehta AK, Zingman BS, Kalil AC, Hohmann E, Chu HY,
156 Luetkemeyer A, Kline S, Lopez de Castilla D, Finberg RW, Dierberg K, Tapson V, Hsieh L,
157 Patterson TF, Paredes R, Sweeney DA, Short WR, Touloumi G, Lye DC, Ohmagari N, Oh M-d,
158 Ruiz-Palacios GM, Benfield T, Fätkenheuer G, Kortepeter MG, Atmar RL, Creech CB, Lundgren J,
159 Babiker AG, Pett S, Neaton JD, Burgess TH, Bonnett T, Green M, Makowski M, Osinusi A, Nayak
160 S, Lane HC. 2020. Remdesivir for the Treatment of Covid-19 — Final Report. New England
161 Journal of Medicine 383:1813-1826.

162 11. Tempestilli M, Caputi P, Avataneo V, Notari S, Forini O, Scorzolini L, Marchioni L, Ascoli Bartoli T,
163 Castilletti C, Lalle E, Capobianchi MR, Nicastri E, D'Avolio A, Ippolito G, Agrati C, Group CIS. 2020.
164 Pharmacokinetics of remdesivir and GS-441524 in two critically ill patients who recovered from
165 COVID-19. J Antimicrob Chemother 75:2977-2980.
166 12. Humeniuk R, Mathias A, Cao H, Osinusi A, Shen G, Chng E, Ling J, Vu A, German P. 2020. Safety,
167 Tolerability, and Pharmacokinetics of Remdesivir, An Antiviral for Treatment of COVID-19, in
168 Healthy Subjects. Clin Transl Sci 13:896-906.
169 13. Shi Y, Shuai L, Wen Z, Wang C, Yan Y, Jiao Z, Guo F, Fu ZF, Chen H, Bu Z, Peng G. 2021. The
170 preclinical inhibitor GS441524 in combination with GC376 efficaciously inhibited the
171 proliferation of SARS-CoV-2 in the mouse respiratory tract. Emerging Microbes & Infections
172 10:481-492.
173 14. Li Y, Cao L, Li G, Cong F, Li Y, Sun J, Luo Y, Chen G, Li G, Wang P, Xing F, Ji Y, Zhao J, Zhang Y, Guo
174 D, Zhang X. 2021. Remdesivir Metabolite GS-441524 Effectively Inhibits SARS-CoV-2 Infection in
175 Mouse Models. J Med Chem doi:10.1021/acs.jmedchem.0c01929.
176 15. Murphy BG, Perron M, Murakami E, Bauer K, Park Y, Eckstrand C, Liepnieks M, Pedersen NC.
177 2018. The nucleoside analog GS-441524 strongly inhibits feline infectious peritonitis (FIP) virus
178 in tissue culture and experimental cat infection studies. Vet Microbiol 219:226-233.
179 16. Pedersen NC, Perron M, Bannasch M, Montgomery E, Murakami E, Liepnieks M, Liu H. 2019.
180 Efficacy and safety of the nucleoside analog GS-441524 for treatment of cats with naturally
181 occurring feline infectious peritonitis. J Feline Med Surg 21:271-281.
182 17. Yan VM, F. 2020. Comprehensive Summary Supporting Clinical Investigation of GS-441524 for
183 Covid-19 Treatment. doi:10.31219, OSFPREPRINTS.
184 18. Schooley RT, Carlin AF, Beadle JR, Valiaeva N, Zhang XQ, Garretson AF, Smith VI, Murphy J,
185 Hostetler KY. 2020. Rethinking Remdesivir: Synthesis of Lipid Prodrugs that Substantially
186 Enhance Anti-Coronavirus Activity. bioRxiv doi:10.1101/2020.08.26.269159.
187 19. Albarino CG, Wiggleton Guerrero L, Lo MK, Nichol ST, Towner JS. 2015. Development of a
188 reverse genetics system to generate a recombinant Ebola virus Makona expressing a green
189 fluorescent protein. Virology 484:259-64.
190 20. Lo MK, Jordan PC, Stevens S, Tam Y, Deval J, Nichol ST, Spiropoulou CF. 2018. Susceptibility of
191 paramyxoviruses and filoviruses to inhibition by 2'-monofluoro- and 2'-difluoro-4'-azidocytidine
192 analogs. Antiviral Res 153:101-113.
193 21. Zhang L, Bukreyev A, Thompson CI, Watson B, Peeples ME, Collins PL, Pickles RJ. 2005. Infection
194 of ciliated cells by human parainfluenza virus type 3 in an in vitro model of human airway
195 epithelium. J Virol 79:1113-24.
196 22. Lo MK, Nichol ST, Spiropoulou CF. 2014. Evaluation of luciferase and GFP-expressing Nipah
197 viruses for rapid quantitative antiviral screening. Antiviral Res 106:53-60.
198 23. Rennick LJ, de Vries RD, Carsillo TJ, Lemon K, van Amerongen G, Ludlow M, Nguyen DT, Yuksel S,
199 Verburgh RJ, Haddock P, McQuaid S, Duprex WP, de Swart RL. 2015. Live-attenuated measles
200 virus vaccine targets dendritic cells and macrophages in muscle of nonhuman primates. J Virol
201 89:2192-200.
202 24. Xu P, Li Z, Sun D, Lin Y, Wu J, Rota PA, He B. 2011. Rescue of wild-type mumps virus from a strain
203 associated with recent outbreaks helps to define the role of the SH ORF in the pathogenesis of
204 mumps virus. Virology 417:126-136.
205 25. Welch SR, Chakrabarti AK, Wiggleton Guerrero L, Jenks HM, Lo MK, Nichol ST, Spiropoulou CF,
206 Albariño CG. 2018. Development of a reverse genetics system for Sosuga virus allows rapid
207 screening of antiviral compounds. PLoS neglected tropical diseases 12:e0006326-e0006326.

208 26. Murray K, Selleck P, Hooper P, Hyatt A, Gould A, Gleeson L, Westbury H, Hiley L, Selvey L,
209 Rodwell B, et al. 1995. A morbillivirus that caused fatal disease in horses and humans. Science
210 268:94-7.
211 27. Harcourt BH, Lowe L, Tamin A, Liu X, Bankamp B, Bowden N, Rollin PE, Comer JA, Ksiazek TG,
212 Hossain MJ, Gurley ES, Breiman RF, Bellini WJ, Rota PA. 2005. Genetic characterization of Nipah
213 virus, Bangladesh, 2004. Emerg Infect Dis 11:1594-7.
214 28. Hallak LK, Spillmann D, Collins PL, Peeples ME. 2000. Glycosaminoglycan sulfation requirements
215 for respiratory syncytial virus infection. J Virol 74:10508-13.
216 29. Welch SR, Guerrero LW, Chakrabarti AK, McMullan LK, Flint M, Bluemling GR, Painter GR, Nichol
217 ST, Spiropoulou CF, Albarino CG. 2016. Lassa and Ebola virus inhibitors identified using
218 minigenome and recombinant virus reporter systems. Antiviral Res 136:9-18.
219 30. Welch SR, Scholte FEM, Flint M, Chatterjee P, Nichol ST, Bergeron É, Spiropoulou CF. 2017.
220 Identification of 2′-deoxy-2′-fluorocytidine as a potent inhibitor of Crimean-Congo hemorrhagic
221 fever virus replication using a recombinant fluorescent reporter virus. Antiviral Research 147:91-
222 99.
223 31. Xie X, Muruato A, Lokugamage KG, Narayanan K, Zhang X, Zou J, Liu J, Schindewolf C, Bopp NE,
224 Aguilar PV, Plante KS, Weaver SC, Makino S, LeDuc JW, Menachery VD, Shi PY. 2020. An
225 Infectious cDNA Clone of SARS-CoV-2. Cell Host Microbe 27:841-848.e3.
226 32. Lo MK, Amblard F, Flint M, Chatterjee P, Kasthuri M, Li C, Russell O, Verma K, Bassit L, Schinazi
227 RF, Nichol ST, Spiropoulou CF. 2020. Potent in vitro activity of β-D-4′-chloromethyl-2′-deoxy-
228 2′-fluorocytidine against Nipah virus. Antiviral Research 175:104712.
229 33. Siegel D, Hui HC, Doerffler E, Clarke MO, Chun K, Zhang L, Neville S, Carra E, Lew W, Ross B,
230 Wang Q, Wolfe L, Jordan R, Soloveva V, Knox J, Perry J, Perron M, Stray KM, Barauskas O, Feng
231 JY, Xu Y, Lee G, Rheingold AL, Ray AS, Bannister R, Strickley R, Swaminathan S, Lee WA, Bavari S,
232 Cihlar T, Lo MK, Warren TK, Mackman RL. 2017. Discovery and Synthesis of a Phosphoramidate
233 Prodrug of a Pyrrolo[2,1-f][triazin-4-amino] Adenine C-Nucleoside (GS-5734) for the Treatment
234 of Ebola and Emerging Viruses. J Med Chem 60:1648-1661.
235 34. Venetsanakos E, Mirza A, Fanton C, Romanov SR, Tlsty T, McMahon M. 2002. Induction of
236 tubulogenesis in telomerase-immortalized human microvascular endothelial cells by
237 glioblastoma cells. Exp Cell Res 273:21-33.
238 35. Reed LJ, Muench H. 1938. A simple method of estimating fifty percent endpoints. Am J Hygiene
239 27:493–497.
240 36. Hostetler KY, Beadle JR, Trahan J, Aldern KA, Owens G, Schriewer J, Melman L, Buller RM. 2007.
241 Oral 1-O-octadecyl-2-O-benzyl-sn-glycero-3-cidofovir targets the lung and is effective against a
242 lethal respiratory challenge with ectromelia virus in mice. Antiviral Res 73:212-8.
243 37. Ramirez RD, Sheridan S, Girard L, Sato M, Kim Y, Pollack J, Peyton M, Zou Y, Kurie JM, Dimaio JM,
244 Milchgrub S, Smith AL, Souza RF, Gilbey L, Zhang X, Gandia K, Vaughan MB, Wright WE, Gazdar
245 AF, Shay JW, Minna JD. 2004. Immortalization of human bronchial epithelial cells in the absence
246 of viral oncoproteins. Cancer Res 64:9027-34.
247 38. Schooley RT, Carlin AF, Beadle JR, Valiaeva N, Zhang X-Q, Clark AE, McMillan RE, Leibel SL,
248 McVicar RN, Xie J, Garretson AF, Smith VI, Murphy J, Hostetler KY. 2021. Rethinking Remdesivir:
249 Synthesis, Antiviral Activity and Pharmacokinetics of Oral Lipid Prodrugs. Antimicrobial Agents
250 and Chemotherapy 0:AAC.01155-21.

251

252

253 FIGURE LEGENDS

254 Figure 1. Comparison of antiviral activities of RVn, RDV, and ODBG-P-RVn in African green monkey (Vero-
255 E6), human hepatoma (Huh7), and human bronchioalveolar carcinoma (NCI-H358) cell lines using
256 reporter-based, image-based, and cytopathic effect (CPE) assays. Representative dose-response
257 inhibition of viral replication and induction of cellular cytotoxicity by RVn (blue shapes), RDV (black
258 shapes), and ODBG-P-RVn (red shapes). A) Direct measurement of reporter fluorescence intensity by
259 recombinant Ebola virus (EBOV) expressing ZsGreen protein in Vero-E6 (left panel) and Huh7 (middle
260 panel) cells, and recombinant Nipah virus (NiV) expressing ZsGreen protein in NCI-H358 (right panel)
261 cells. B) Image-based counting of reporter fluorescence-positive cells infected with recombinant severe
262 acute respiratory syndrome coronavirus 2 (SARS-CoV-2) expressing mNeonGreen protein (Vero-E6 and
263 Huh7) and recombinant respiratory syncytial virus (RSV) expressing eGFP (NCI-H358). Infected cells
264 treated with DMSO were considered as 100% fluorescence intensity signal and 100% fluorescence-
265 positive cell counts. C) Compound-based inhibition of CPE induced by yellow fever virus (YFV) in Vero-E6
266 and Huh7 cells and by Hendra virus (HeV) in NCI-H358 cells determined by measuring cellular ATP levels
267 (CellTiterGlo 2.0). ATP levels in uninfected cells treated with DMSO were considered 100% CPE
268 inhibition. D) Compound cytotoxicity/cell viability measured by CellTiterGlo 2.0 assay. Dose-response
269 curves were fitted to the mean value of experiments performed in biological triplicate for each
270 concentration in the 8-point, 3-fold dilution series using a 4-parameter non-linear logistic regression
271 curve with variable slope. Data points and error bars indicate the mean value and standard deviation of
272 3 biological replicates; each colored shape/line in the legend represents an independent experiment
273 performed in biological triplicate. RVn and RDV used in this study was obtained from MedChemExpress
274 (Monmouth Junction, NJ USA).

275 Figure 2. Comparison of cell type-dependent antiviral activities of RVn, RDV, and ODBG-P-RVn in
276 primary-like hTERT-immortalized microvascular endothelial (TIME) cells and small airway epithelial cells

277 (HSAEC1-KT). A) Representative dose-response inhibition of recombinant EBOV, NiV, and Marburg virus
278 (MARV) expressing ZsGreen protein in TIME cells. B) Yield reduction of infectious EBOV-ZsG (left panel)
279 and NiV-ZsG (middle panel) by RDV and ODBG-P-RVn. Compound cytotoxicity/cell viability (right panel)
280 in TIME cells measured via CellTiterGlo 2.0 assay. C) Representative dose-response inhibition of
281 recombinant EBOV, NiV, and MARV expressing ZsGreen protein in HSAEC1-KT cells. D) Reduction of
282 infectious yield of EBOV-ZsG (left panel) and NiV-ZsG (middle panel) by RDV and ODBG-P-RVn in
283 HSAEC1-KT cells. Compound cytotoxicity/cell viability (right panel) in HSAEC1-KT cells measured via
284 CellTiterGlo 2.0 assay. Dose-response curves were fitted to the mean value of experiments performed in
285 biological triplicate for each concentration in the 8-point, 3-fold dilution series using a 4-parameter non-
286 linear logistic regression curve with variable slope. Data points and error bars indicate the mean value
287 and standard deviation of 3 or 4 biological replicates; each colored shape/line in the legend represents
288 an independent experiment performed in biological triplicate. Infectious yield reduction assays were
289 conducted once with biological quadruplicates.

290 SUPPLEMENTAL FIGURE LEGENDS

291 Supplemental Figure S1. Comparison of antiviral activities of RVn, RDV, and ODBG-P-RVn in African
292 green monkey (Vero-E6) cells using reporter-based, image-based, and CPE assays. Representative dose-
293 response inhibition of virus replication by RVn (blue shapes), RDV (black shapes), and ODBG-P-RVn (red
294 shapes). Signal from infected cells treated with DMSO served as 100% fluorescence intensity signal for
295 reporter assays and 100% fluorescence-positive cell counts for image-based assays. CPE inhibition was
296 measured by determining cellular ATP levels using CellTiterGlo 2.0 assay reagent. ATP levels in
297 uninfected cells treated with DMSO served as 100% CPE inhibition. Dose-response curves were fitted to
298 the mean value of experiments performed in biological triplicate for each concentration in the 8-point,
299 3-fold dilution series using a 4-parameter non-linear logistic regression curve with variable slope. Data
300 points and error bars indicate the mean value and standard deviation of 3 biological replicates; each

301 colored shape/line in the legend represents an independent experiment performed in biological
302 triplicate.

303 Supplemental Figure S2. Comparison of antiviral activities of RVn, RDV, and ODBG-P-RVn in Huh7 cells
304 using reporter-based, image-based, and CPE assays. Representative dose-response inhibition of virus
305 replication by RVn (blue shapes), RDV (black shapes), and ODBG-P-RVn (red shapes). Signal from
306 infected cells treated with DMSO served as 100% fluorescence intensity signal for reporter assays and
307 100% fluorescence-positive cell counts for image-based assays. CPE inhibition was measured by
308 determining cellular ATP levels using CellTiterGlo 2.0 assay reagent. ATP levels in uninfected cells
309 treated with DMSO served as 100% CPE inhibition. Dose-response curves were fitted to the mean value
310 of experiments performed in biological triplicate for each concentration in the 8-point, 3-fold dilution
311 series using a 4-parameter non-linear logistic regression curve with variable slope. Data points and error
312 bars indicate the mean value and standard deviation of 3 biological replicates; each colored shape/line
313 in the legend represents an independent experiment performed in biological triplicate.

314 Supplemental Figure S3. Comparison of antiviral activities of RVn, RDV, and ODBG-P-RVn in human
315 bronchioalveolar carcinoma (NCI-H358) cells using reporter-based, image-based, and CPE assays.
316 Representative dose-response inhibition of virus replication by RVn (blue shapes), RDV (black shapes),
317 and ODBG-P-RVn (red shapes). Signal in infected cells treated with DMSO served as 100% fluorescence
318 intensity signal for reporter assays and 100% fluorescence-positive cell counts for image-based assays.
319 CPE inhibition was measured by determining cellular ATP levels using CellTiterGlo 2.0 assay reagent. ATP
320 levels in uninfected cells treated with DMSO served as 100% CPE inhibition. Dose-response curves were
321 fitted to the mean value of experiments performed in biological triplicate for each concentration in the
322 8-point, 3-fold dilution series using a 4-parameter non-linear logistic regression curve with variable
323 slope. Data points and error bars indicate the mean value and standard deviation of 3 biological

324 replicates; each colored shape/line in the legend represents an independent experiment performed in
325 biological triplicate.

326 Supplemental Figure S4. Comparison of antiviral activities of RVn, RDV, and ODBG-P-RVn in primary-like
327 human small airway epithelial (HSAEC1-KT) cells using reporter-based, image-based, and CPE assays.
328 Representative dose-response inhibition of virus replication by RVn (blue shapes), RDV (black shapes),
329 and ODBG-P-RVn (red shapes). Signal in infected cells treated with DMSO served as 100% fluorescence
330 intensity signal for reporter assays and 100% fluorescence-positive cell counts for image-based assays.
331 CPE inhibition was measured by determining cellular ATP levels using CellTiterGlo 2.0 assay reagent. ATP
332 levels in uninfected cells treated with DMSO served as 100% CPE inhibition. Dose-response curves were
333 fitted to the mean value of experiments performed in biological triplicate for each concentration in the
334 8-point, 3-fold dilution series using a 4-parameter non-linear logistic regression curve with variable
335 slope. Data points and error bars indicate the mean value and standard deviation of 3 biological
336 replicates; each colored shape/line in the legend represents an independent experiment performed in
337 biological triplicate.

Table 1. Mean antiviral activity of RVn, RDV, and ODBG-P-RVn in Vero E6, Huh7, and NCI-H358 cell lines

				Vero E6									Huh7/NCI-H358								
				RVn (GS-441524)			RDV (GS-5734)			ODBG-P-RVn			RVn (GS-441524)			RDV (GS-5734)			ODBG-P-RVn		
Virus Family	**Virus**	**Species/Variant**	**Assay**	**EC_{50}**	**EC_{90}**	**SI (CC_{50}: >100)**	**EC_{50}**	**EC_{90}**	**SI (CC_{50}: >100)**	**EC_{50}**	**EC_{90}**	**SI (CC_{50}: >100)**	**EC_{50}**	**EC_{90}**	**SI (CC_{50}: >100/ >100)**	**EC_{50}**	**EC_{90}**	**SI (CC_{50}: 54.2 ± 6.0/ 77.2 ± 5.3)**	**EC_{50}**	**EC_{90}**	**SI (CC_{50}: 93.4 ± 3.0/ >100)**
Filoviridae	EBOV	Rec. Makona-ZsG	REP	2.03 ± 0.50	7.54 ± 1.09	49	5.15 ± 1.09	17.31 ± 0.89	>19	0.39 ± 0.10	1.71 ± 0.25	>258	1.84 ± 0.31	6.91 ± 1.79	>54	0.020 ± 0.003	0.16 ± 0.02	2710	0.37 ± 0.06	2.13 ± 0.37	251
	MARV	Rec. Bat371-ZsG	REP	0.96 ± 0.09	4.05 ± 1.42	104	2.16 ± 0.27	10.22 ± 2.02	>46	0.19 ± 0.04	0.81 ± 0.12	>521	1.92 ± 0.06	4.47 ± 0.48	>52	0.025 ± 0.002	0.075 ± 0.003	2128	0.33 ± 0.02	0.99 ± 0.09	285
Paramxyovirdae	NiV-M	Rec. Malaysia-ZsG	REP	1.10 ± 0.40	2.20 ± 1.05	73	5.87 ± 0.19	9.82 ± 0.43	>16	0.31 ± 0.04	0.78 ± 0.28	>196	2.43 ± 0.31	5.95 ± 1.10	>41	0.075 ± 0.001	0.31 ± 0.04	1026	0.50 ± 0.06	2.83 ± 1.39	>198
			CPE	0.48 ± 0.06	0.78 ± 0.19	207	3.34 ± 0.34	5.39 ± 0.29	>30	0.19 ± 0.01	0.30 ± 0.04	>522	ND	ND	N/A	ND	ND	N/A	ND	ND	N/A
	NiV-B	Bangladesh	CPE	0.52 ± 0.02	1.14 ± 0.02	192	2.84 ± 0.10	5.81 ± 0.44	>35	0.17 ± 0.01	0.38 ± 0.04	>599	3.42 ± 0.005	5.41 ± 0.29	>29	0.12 ± 0.0004	0.19 ± 0.01	661	0.82 ± 0.053	1.38 ± 0.05	>122
	HeV	1996	CPE	1.43 ± 0.17	12.06 ± 3.14	70	4.56 ± 0.20	17.58 ± 3.91	>22	0.37 ± 0.04	3.93 ± 1.98	>270	3.68 ± 0.08	6.33 ± 0.18	>27	0.16 ± 0.02	0.25 ± 0.03	491	0.95 ± 0.12	1.42 ± 0.03	>105
	MV	Rec. $rMV^{EZ}GFP(3)$	REP	0.58 ± 0.20	1.71 ± 0.07	172	4.97 ± 0.25	6.12 ± 0.3	>20	0.16 ± 0.03	0.21 ± 0.01	>609	0.88 ± 0.16	6.99 ± 1.90	>113	0.025 ± 0.007	0.13 ± 0.09	3074	0.12 ± 0.003	0.86 ± 0.22	>803
	hPIV3	Rec. JS-GFP	FFU	0.14 ± 0.01	0.28 ± 0.02	70	0.43 ± 0.09	0.90 ± 0.03	>232	0.026 ± 0.002	0.050 ± 0.002	>3896	1.43 ± 0.16	1.98 ± 0.05	>70	0.031 ± 0.002	0.052 ± 0.01	2458	0.22 ± 0.01	0.43 ± 0.02	>457
	MuV	Rec. IA2006-eGFP	FFU	5.11 ± 0.20	7.80 ± 0.64	18	16.81 ± 1.23	25.1 ± 1.97	>4.9	1.13 ± 0.04	2.53 ± 0.25	>56	9.3 ± 0.30	13.71 ± 0.24	>11	0.20 ± 0.003	0.24 ± 0.003	266	1.85 ± 0.11	2.24 ± 0.23	50
	SoSuV	Rec. 2012-ZsG	REP	1.00 ± 0.10	2.72 ± 0.62	100	5.31 ± 1.8	19.10 ± 9.31	>19	0.31 ± 0.089	0.80 ± 0.06	>325	2.06 ± 0.09	7.76 ± 1.11	>48	0.052 ± 0.01	0.13 ± 0.02	1042	0.52 ± 0.10	1.08 ± 0.15	180
Pneumoviridae	RSV	Rec. rgRSV0224 (A2)	FFU	0.49 ± 0.05	0.62 ± 0.01	206	1.80 ± 0.08	2.40 ± 0.27	>55	0.10 ± 0.02	0.22 ± 0.03	>997	1.93 ± 0.02	2.36 ± 0.08	>51	0.078 ± 0.004	0.17 ± 0.02	991	0.55 ± 0.057	1.41 ± 0.09	>180
Coronaviridae	SARS-CoV-2	Rec. icSARS-CoV-2 mNG (WA1)	FFU	0.42 ± 0.09	0.60 ± 0.06	236	1.77 ± 0.13	2.81 ± 0.78	>56	0.10 ± 0.005	0.16 ± 0.01	>997	0.69 ± 0.01	1.50 ± 0.20	>144	0.011 ± 0.001	0.035 ± 0.002	5073	0.12 ± 0.02	0.69 ± 0.07	778
Flaviviridae	YFV	17D	CPE	3.52 ± 0.24	30.25 ± 10.08	28	19.86 ± 1.73	>50	>5	0.87 ± 0.043	7.37 ± 1.59	>114	36.83 ± 2.85	>50	>2.7	0.88 ± 0.057	3.09 ± 1.47	62	14.11 ± 0.90	>50	6.6
Arenaviridae	LASV	Rec. Josiah-ZsG	REP	NI	NI	N/A	NI	NI	N/A	31.14 ± 7.79	>50	>3	NI	NI	N/A	2.87 ± 0.61	5.17 ± 0.33	19	NI	NI	N/A
Nairoviridae	CCHF	Rec. IbAr10200-ZsG	REP	NI	NI	N/A	NI	NI	N/A	NI	NI	N/A	NI	NI	N/A	NI	NI	N/A	NI	NI	N/A

EC_{50}, 50% effective inhibition concentration; EC_{90}, 90% effective inhibition concentration; CC_{50}, 50% cytotoxic concentration; SI, selective index = EC_{50}/CC_{50}; REP, reporter; CPE, cytopathic effect; FFU, focus-forming unit; ND, not determined; NI, no inhibition; N/A, not applicable; Rec, recombinant. Mean values with ± standard deviation values were derived from 3 independent experiments performed in biological triplicates except for NiV-B (NCI-H358), HeV (NCI-H358), and YFV (Vero E6)which were performed twice in biological triplicates. Data in red text derived from Huh7 cells, data in blue derived from NCI-H358 cells. REP/FFU/CPE assays were conducted between 72-144 hpi. EC_{50}, EC_{90}, and CC_{50} values were calculated using Graphpad Prism 9 software.

Table 2. Mean antiviral activity of RVn, RDV, and ODBG-P-RVn in primary-like hTERT-immortalized microvascular endothelial (TIME) and small airway epithelial (HSAEC1-KT) cell lines

				HSAEC1-KT									TIME								
				RVn (GS-441524)			RDV (GS-5734)			ODBG-P-RVn			RVn (GS-441524)			RDV (GS-5734)			ODBG-P-RVn		
Virus Family	**Virus**	**Species/Variant**	**Assay**	**EC_{50}**	**EC_{90}**	**SI (CC_{50}: >100)**	**EC_{50}**	**EC_{90}**	**SI (CC_{50}: >100)**	**EC_{50}**	**EC_{90}**	**SI (CC_{50}: 20.5 ± 0.29)**	**EC_{50}**	**EC_{90}**	**SI (CC_{50}: >100)**	**EC_{50}**	**EC_{90}**	**SI (CC_{50}: 17.2 ± 0.42)**	**EC_{50}**	**EC_{90}**	**SI (CC_{50}: >50)**
Filoviridae	EBOV	Rec. Makona-ZsG	REP	10.7 ± 2.62	21.79 ± 3.16	>9.3	0.17 ± 0.02	0.41 ± 0.14	>587	0.21 ± 0.02	1.06 ± 0.18	98	14.88 ± 0.28	17.24 ± 0.16	>3.36	0.13 ± 0.04	0.2 ± 0.01	132	0.99 ± 0.063	1.96 ± 0.043	>50
			VTR	ND	ND	N/A	0.11	0.82	>909	0.21	0.95	98	ND	ND	N/A	0.032	0.064	530	0.15	0.39	>324
	MARV	Rec. Bat371-ZsG	REP/FFU	35.53 ± 7.07	71.35 ± 1.28	>2.8	0.75 ± 0.19	2.92 ± 0.14	>133	0.71 ± 0.11	3.67 ± 0.49	29	5.2 ± 0.26	6.89 ± 0.86	>9.61	0.04 ± 0.003	0.086 ± 0.004	430	0.23 ± 0.036	0.66 ± 0.032	>213
Paramxyovirdae	NiV-M	Rec. Malaysia-ZsG	REP	16.46 ± 0.04	19.12 ± 0.05	>6.1	0.23 ± 0.01	0.31 ± 0.06	>440	0.57 ± 0.013	0.97 ± 0.21	36	13.53 ± 2.44	17.52 ± 0.77	>3.70	0.10 ± 0.01	0.20 ± 0.01	172	0.75 ± 0.05	2.01 ± 0.30	>66
			CPE	16.12 ± 4.21	78.1 ± 35.08	>6.2	0.31 ± 0.04	0.075 ± 0.004	>318	0.90 ± 0.07	10.22 ± 4.99	23	ND	ND	N/A	0.054	0.07	319	0.26	0.77	>195
			VTR	ND	ND	N/A	0.26	0.36	>379	0.47	0.77	44									
	NiV-B	Bangladesh	CPE	11.23 ± 0.63	33.6 ± 1.58	>8.9	0.21 ± 0.063	0.62 ± 0.20	>379	0.41 ± 0.039	1.71 ± 0.66	50									
	HeV	1994	CPE	11.52 ± 1.49	26.11 ± 4.44	>8.7	0.22 ± 0.04	0.65 ± 0.11	>463	0.42 ± 0.023	1.19 ± 0.061	49									
	MV	Rec. $rMV^{EZ}GFP(3)$	REP	4.98 ± 0.37	12.02 ± 2.7	>20	0.063 ± 0.02	0.128 ± 0.016	>1587	0.082 ± 0.026	0.29 ± 0.043	251									
	hPIV3	Rec. JS-GFP	FFU	4.96 ± 0.05	5.77 ± 0.06	>20	0.063 ± 0.001	0.074 ± 0.002	>1582	0.091 ± 0.009	0.20 ± 0.008	226									
Pneumoviridae	RSV	Rec. rgRSV0224 (A2)	FFU	4.92 ± 0.47	8.09 ± 0.68	>20	0.088 ± 0.026	0.21 ± 0.033	>1134	0.12 ± 0.008	0.34 ± 0.047	176									

EC_{50}, 50% effective inhibition concentration; EC_{90}, 90% effective inhibition concentration; CC_{50}, 50% cytotoxic concentration; SI, selective index = EC_{50}/CC_{50}; REP, reporter; CPE, cytopathic effect; FFU, focus-forming unit; VTR, virus titer reduction; ND, not determined; N/A, not applicable; Rec, recombinant. Mean values with ± standard deviation values were derived from a minimum of 3 independent experiments performed in biological triplicates. REP/FFU/CPE/VTR assays were conducted at 72 hpi. EC_{50}, EC_{90}, and CC_{50} values were calculated using Graphpad Prism 9 software.

Figure 1.

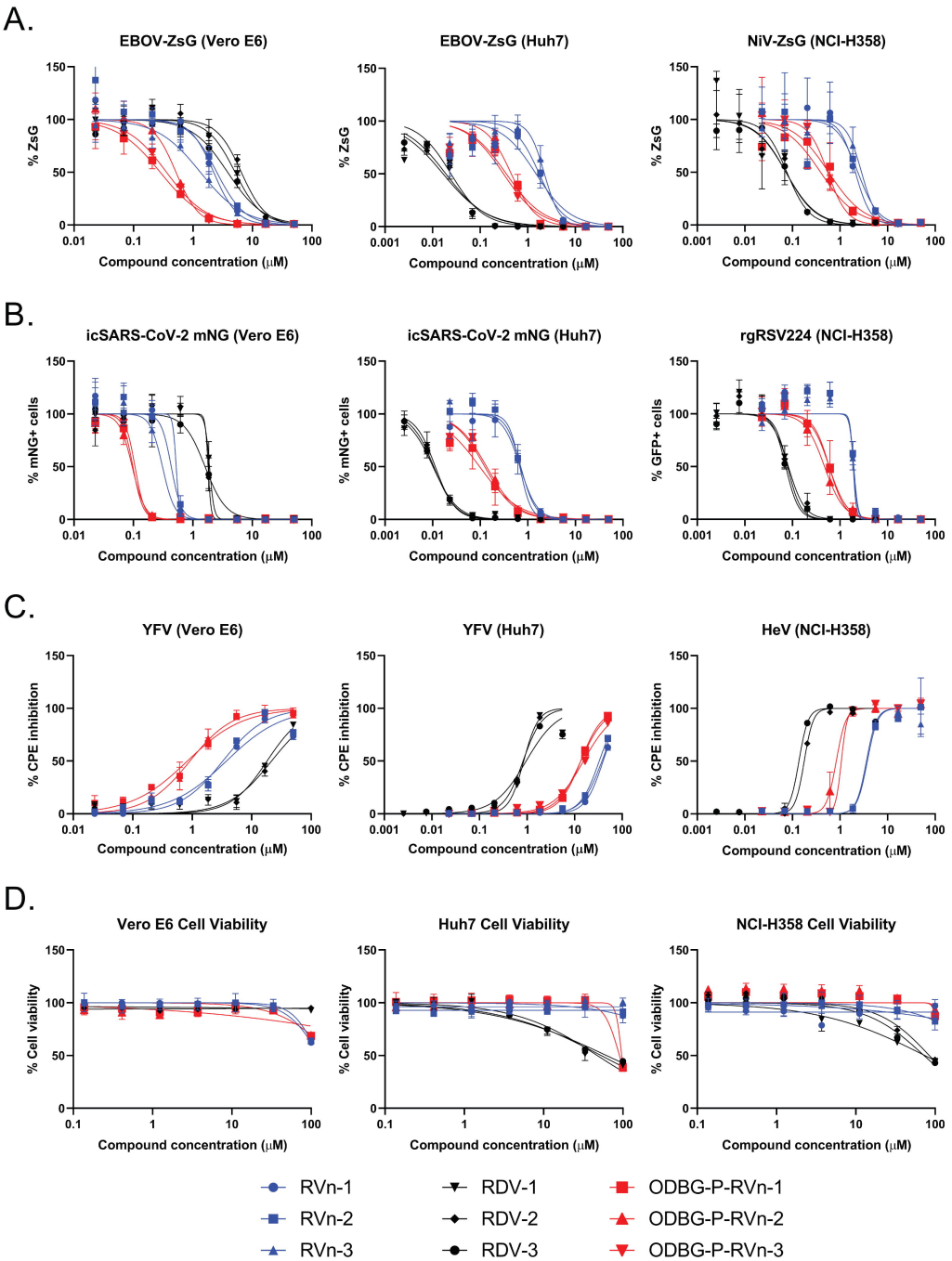

Figure 1. Comparison of antiviral activities of RVn, RDV, and ODBG-P-RVn in African green monkey (Vero E6), Human hepatoma (Huh7), and human bronchioalveolar carcinoma (NCI-H358) cell lines using reporter-based, image-based, and cytopathic effect assays. Representative dose response inhibition of virus replication and induction of cell cytotoxicity in by RVn (blue shapes), RDV (black shapes), and ODBG-P-RVn (red shapes). A) Direct measurement of green fluorescence reporter intensity by recombinant EBOV expressing ZsGreen protein in Vero E6 (left panel) and Huh7 (middle panel) cells, and recombinant NiV expressing ZsGreen protein in NCI-H358 (right panel) cells. B) Image-based counting of reporter fluorescence-positive cells infected with recombinant SARS-CoV-2 expressing mNeonGreen protein (Vero E6 and Huh7) and recombinant RSV expressing eGFP (NCI-H358). Infected cells treated with DMSO represented 100% fluorescence intensity signal and 100% fluorescence-positive cell counts. C) Inhibition of cytopathic effect (CPE) by YFV (Vero E6 and Huh7) and HeV (NCI-H358) measured by levels of cellular ATP (CellTiterGlo 2.0). Uninfected cells treated with DMSO served as 100% CPE inhibition. D) Compound cytotoxicity/cell viability measured by CellTiterGlo 2.0 assay. Dose response curves were fitted to the mean value of experiments performed in biological triplicate for each concentration in the 8-point 3-fold dilution series using a 4-parameter non-linear logistic regression curve with variable slope. Data points and error bars indicate the mean value and standard deviation of 3 biological replicates; each colored shape/line in the legend represents an independent experiment performed in biological triplicate.

Figure 2.

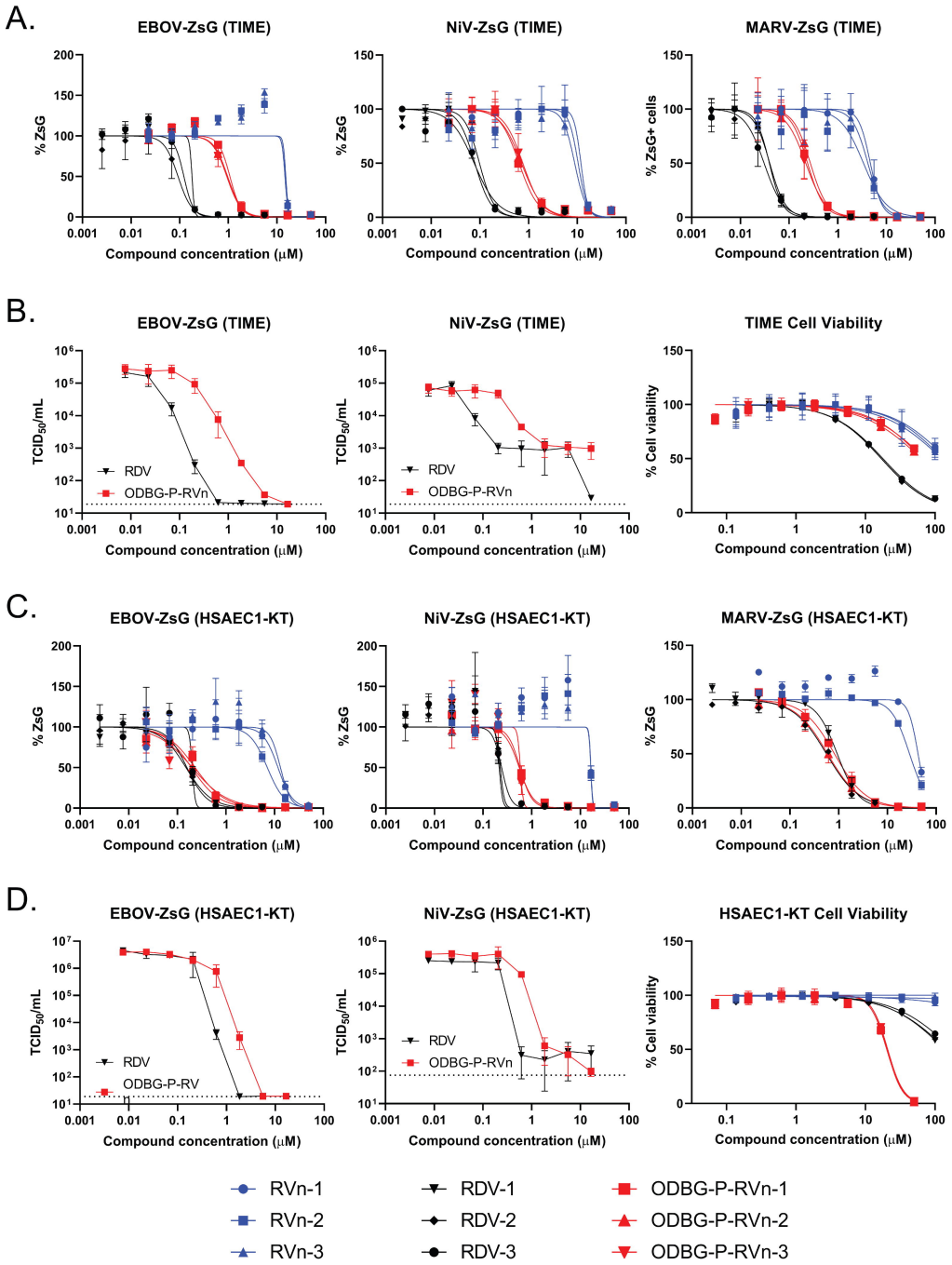

Figure 2. Comparison of cell-type dependent antiviral activities of RVn, RDV, and ODBG-P-RVn in primary-like hTERT-immortalized microvascular endothelial (TIME) and small airway epithelial cells (HSAEC1-KT). A) Representative dose response inhibition of recombinant EBOV, NiV, and MARV expressing ZsGreen protein in TIME cells. B) Infectious yield reduction by RDV and ODBG-P-RVn against EBOV-ZsG (left panel) and NiV-ZsG (middle panel). Compound cytotoxicity/cell viability (right panel) in TIME cells measured by CellTiterGlo 2.0 assay. C) Representative dose response inhibition of recombinant EBOV, NiV, and MARV expressing ZsGreen protein in HSAEC1-KT cells. (D) Infectious yield reduction by RDV and ODBG-P-RVn against EBOV-ZsG (left panel) and NiV-ZsG (middle panel) in HSAEC1-KT cells. Compound cytotoxicity/cell viability (right panel) in HSAEC1-KT cells measured by CellTiterGlo 2.0 assay. Dose response curves were fitted to the mean value of experiments performed in biological triplicate for each concentration in the 8-point 3-fold dilution series using a 4-parameter non-linear logistic regression curve with variable slope. Data points and error bars indicate the mean value and standard deviation of 3 or 4 biological replicates; each colored shape/line in the legend represents an independent experiment performed in biological triplicate. Infectious yield reduction assays were conducted once with biological quadruplicates.

S1.

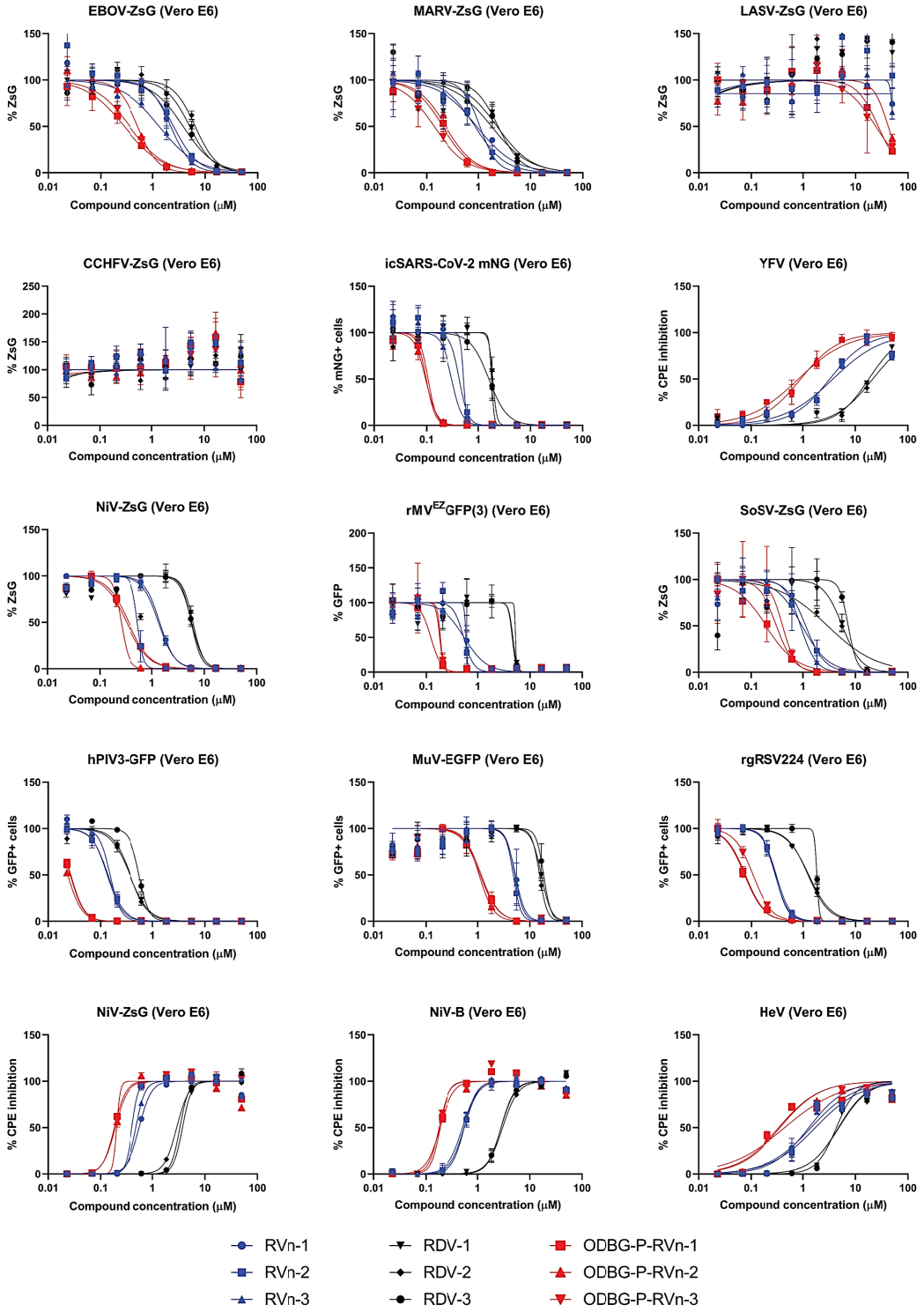

Supplemental Figure S1. Comparison of antiviral activities of RVn, RDV, and ODBG-P-RVn in African green monkey (Vero E6) cells using reporter-based, image-based, and cytopathic effect assays. Representative dose response inhibition of virus replication by RVn (blue shapes), RDV (black shapes), and ODBG-P-RVn (red shapes). Infected cells treated with DMSO served as 100% fluorescence intensity signal for reporter assays and 100% fluorescence-positive cell counts for image-based assays. Inhibition of cytopathic effect was measured by levels of cellular ATP using CellTiterGlo 2.0 assay reagent (Promega, WI). Uninfected cells treated with DMSO served as 100% CPE inhibition. Dose response curves were fitted to the mean value of experiments performed in biological triplicate for each concentration in the 8-point 3-fold dilution series using a 4-parameter non-linear logistic regression curve with variable slope. Data points and error bars indicate the mean value and standard deviation of 3 biological replicates; each colored shape/line in the legend represents an independent experiment performed in biological triplicate.

S2.

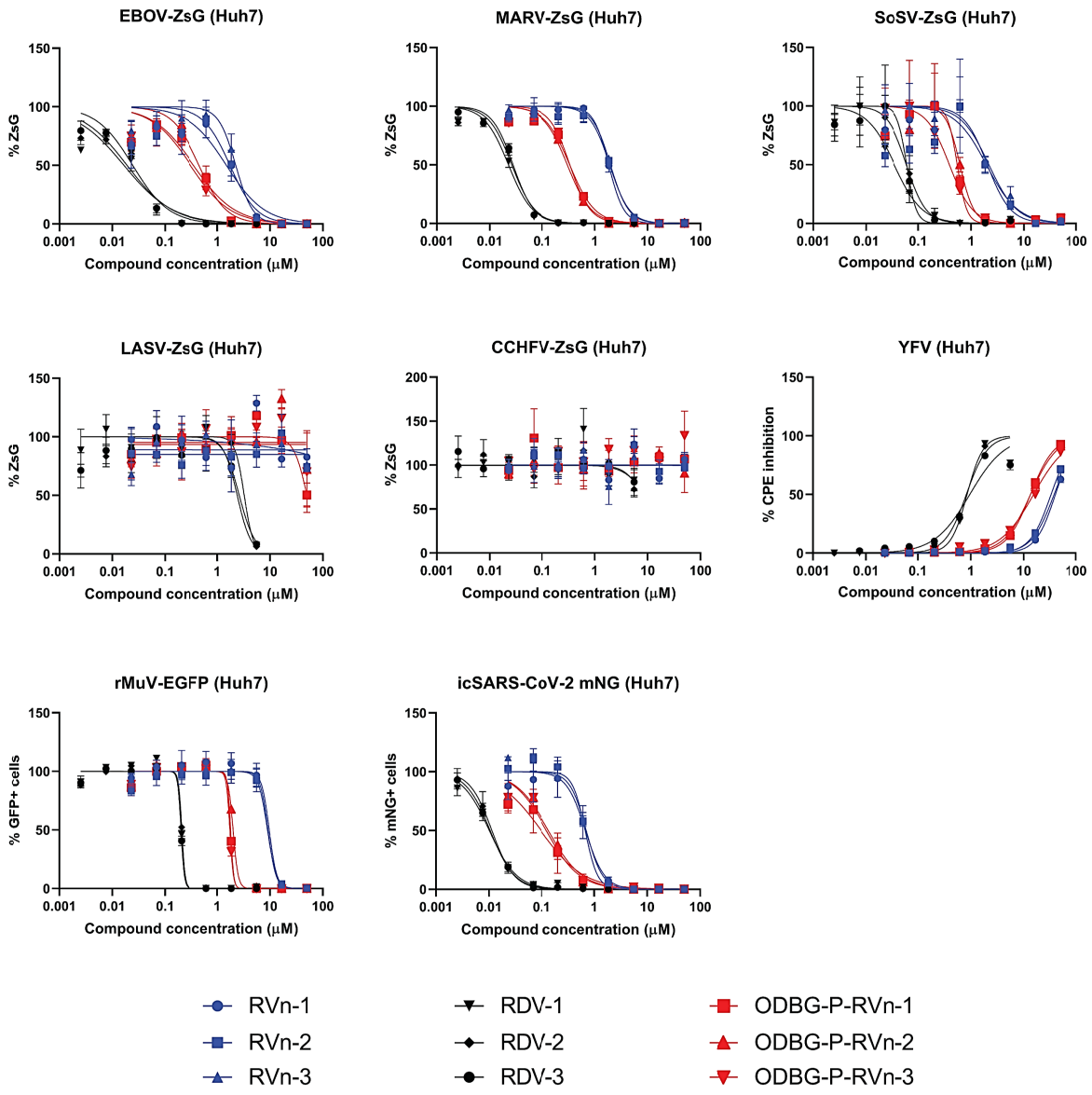

Supplemental Figure S2. Comparison of antiviral activities of RVn, RDV, and ODBG-P-RVn in human hepatoma (Huh7) cells using reporter-based, image-based, and cytopathic effect assays. Representative dose response inhibition of virus replication by RVn (blue shapes), RDV (black shapes), and ODBG-P-RVn (red shapes). Infected cells treated with DMSO served as 100% fluorescence intensity signal for reporter assays and 100% fluorescence-positive cell counts for image-based assays. Inhibition of cytopathic effect was measured by levels of cellular ATP using CellTiterGlo 2.0 assay reagent (Promega, WI). Uninfected cells treated with DMSO served as 100% CPE inhibition. Dose response curves were fitted to the mean value of experiments performed in biological triplicate for each concentration in the 8-point 3-fold dilution series using a 4-parameter non-linear logistic regression curve with variable slope. Data points and error bars indicate the mean value and standard deviation of 3 biological replicates; each colored shape/line in the legend represents an independent experiment performed in biological triplicate.

S3.

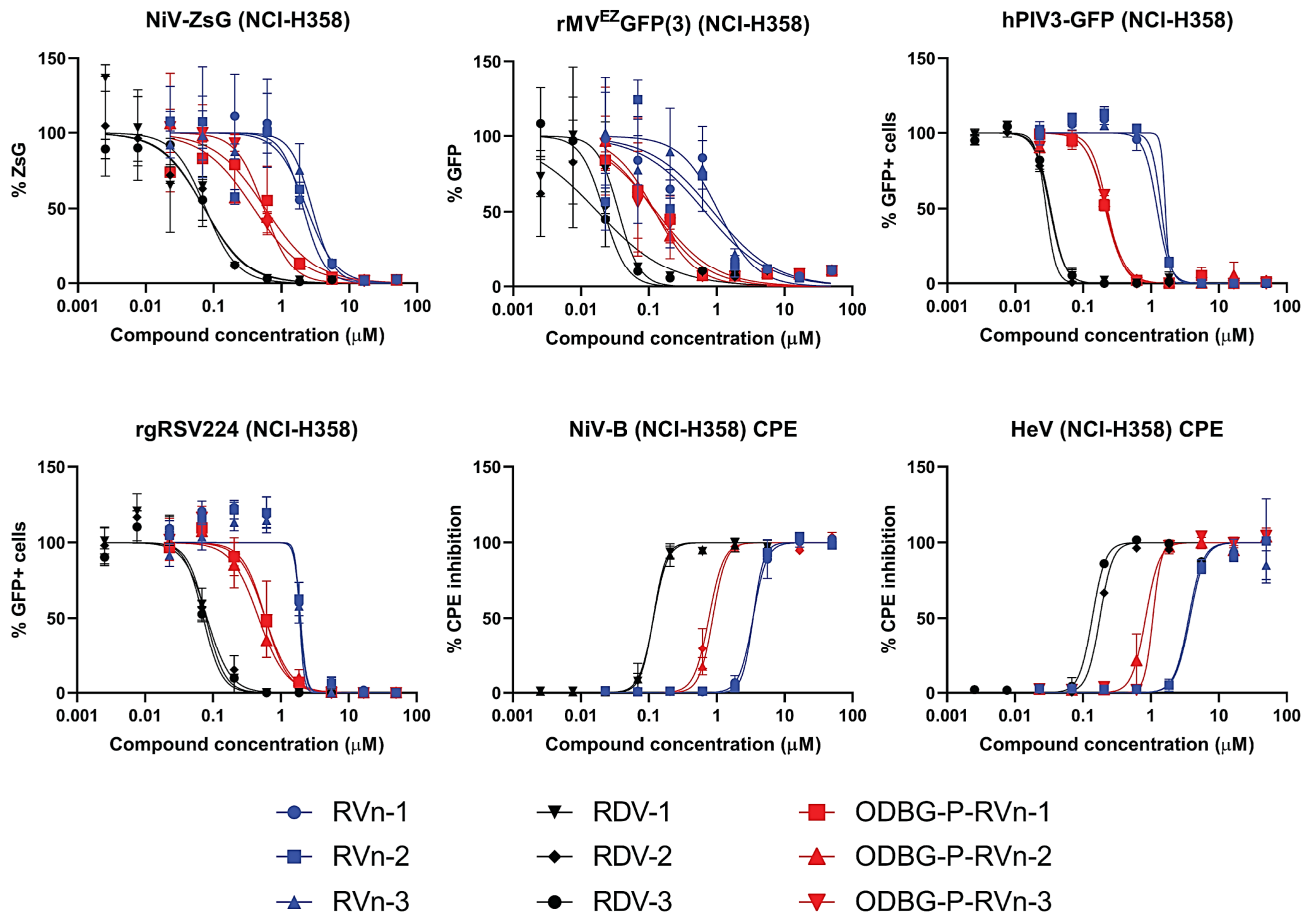

Supplemental Figure S3. Comparison of antiviral activities of RVn, RDV, and ODBG-P-RVn in human bronchioalveolar carcinoma (NCI-H358) cells using reporter-based, image-based, and cytopathic effect assays. Representative dose response inhibition of virus replication by RVn (blue shapes), RDV (black shapes), and ODBG-P-RVn (red shapes). Infected cells treated with DMSO served as 100% fluorescence intensity signal for reporter assays and 100% fluorescence-positive cell counts for image-based assays. Inhibition of cytopathic effect was measured by levels of cellular ATP using CellTiterGlo 2.0 assay reagent (Promega, WI). Uninfected cells treated with DMSO served as 100% CPE inhibition. Dose response curves were fitted to the mean value of experiments performed in biological triplicate for each concentration in the 8-point 3-fold dilution series using a 4-parameter non-linear logistic regression curve with variable slope. Data points and error bars indicate the mean value and standard deviation of 3 biological replicates; each colored shape/line in the legend represents an independent experiment performed in biological triplicate.

S4.

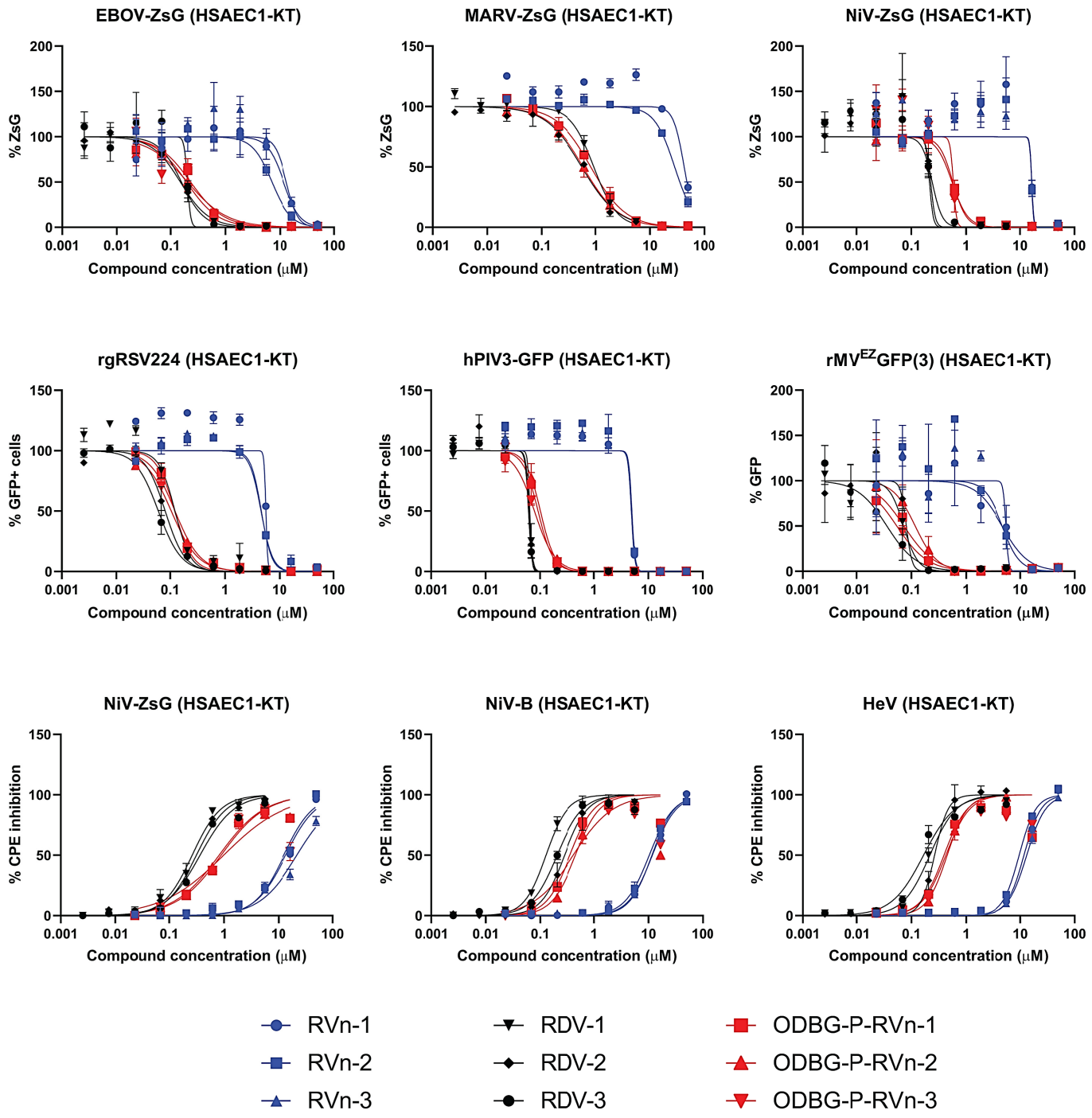

Supplemental Figure S4. Comparison of antiviral activities of RVn, RDV, and ODBG-P-RVn in primary-like human small airway epithelial (HSAEC1-KT) cells using reporter-based, image-based, and cytopathic effect assays. Representative dose response inhibition of virus replication by RVn (blue shapes), RDV (black shapes), and ODBG-P-RVn (red shapes). Infected cells treated with DMSO served as 100% fluorescence intensity signal for reporter assays and 100% fluorescence-positive cell counts for image-based assays. Inhibition of cytopathic effect was measured by levels of cellular ATP using CellTiterGlo 2.0 assay reagent (Promega, WI). Uninfected cells treated with DMSO served as 100% CPE inhibition. Dose response curves were fitted to the mean value of experiments performed in biological triplicate for each concentration in the 8-point 3-fold dilution series using a 4-parameter non-linear logistic regression curve with variable slope. Data points and error bars indicate the mean value and standard deviation of 3 biological replicates; each colored shape/line in the legend represents an independent experiment performed in biological triplicate.